IEEE Access
Multidisciplinary | Rapid Review | Open Access Journal

Received November 7, 2019, accepted November 30, 2019, date of publication January 7, 2020, date of current version January 27, 2020.

Digital Object Identifier 10.1109/ACCESS.2020.2964664

A Novel Method for Determination on Switch Timing Between Damping and Non-Damping Status of Strapdown Fiber Optic Gyrocompass

YANG LIU, GONGLIU YANG, AND QINGZHONG CAI
School of Instrumentation and Optoelectronic Engineering, Beihang University, Beijing 100191, China

Corresponding author: Qingzhong Cai (qingzhong_cai@163.com)

This work was supported in part by the National Natural Science Foundation of China under Grant 61803015 and Grant 61374210, in part by the National Key Research and Development Program of China under Grant 2016YFB0501600, and in part by the National Equipment Pre-Research Foundation under Grant 6140517020101.

ABSTRACT It is necessary to locate the precise timing of switching into non-damping mode when the ship comes across zigzag maneuver, which helps avoid overshoot errors and maintain accuracy of ship's attitudes. In this paper, we propose a novel method to make the right decision on the damping/non-damping switch timing selection. Ship's in-motion data, collected by the gyrocompass system in advance, will first be pre-processed using wavelet denoising procedure and then treat as support vector machine (SVM) training in-put. Once the model is established, strapdown fiber optic gyrocompass (FOGC) can be equipped with the ability of self-judgment on when to cut off the alignment closed loops to become invulnerable and when to let it back online to remain stable by means of SVM classification schemes for switch timing recognition. Results show our method has better performance in the time of ships maneuver compared to the whole course damping network solution. Furthermore, transverse comparisons indicate our Wavelet-SVM method has better performance than BP neural network and traditional threshold method during maneuvering navigation process.

INDEX TERMS Strapdown gyrocompass, alignment loops, switch timing, support vector machine, wavelet denoising.

I. INTRODUCTION

Ship navigation is necessary for the long voyage. On-board equipment should continuously provide accurate information for the helmsman, such as roll, pitch, heading angles, to ensure the vessel voyage along the predetermined course. Nowadays inertial navigation system (INS) integrated with SPEED LOG is one of typical navigation methods and well applied in most surface ships and submarines [1]–[3]. In practice, due to high cost and cubage of traditional INS, it makes the system difficult to install and upgrade. With the rapid development of strapdown navigation technology, a new generation of navigation products begin appear. Strapdown fiber optic gyrocompass (FOGC), which normally consists of three-axis orthogonal fiber optic gyroscopes and quartz accelerometers, can provide position, attitude, velocity and angular velocity information for ships [4]–[6]. Besides, FOGC's compact structure, low power consumption and less maintenance made it of high stability and show good prospects for application [7]. So far FOGC can enable autonomous underwater vehicles (AUVs) and remotely controlled underwater vehicles (ROVs) to handle high-end missions such as seafloor imaging, mine countermeasures, mineral deposits, etc [8], [9].

FOGC can provide in-time attitudes of the ship thanks to the involvement of the gyrocompass alignment loops. This kind of closed loop design eliminates Schuler oscillation in the pure inertial navigation system and indeed prevents velocity, attitude and position errors accumulating over time [4]. However, the break of the period of Schuler oscillation means being vulnerable to outside interference. When the ship is in fast-motion mode, like turning maneuver, heading angles shown from FOGC will drift off the correct course and it will take several periods of oscillation to settle down [11], [12]. Until now many researchers have focused on the modification of the damping network.

The associate editor coordinating the review of this manuscript and approving it for publication was Huiling Chen.

In Reference [10], electromagnetic log (EM-log) is used to track the maneuver velocity of the vessel and remove the earth rotation angular velocity and the angular velocity of the navigation frame relative to the earth frame from accelerometer measurements. By changing the structure of gyrocompass alignment loop, EM-log measurements can also be employed to reduce the negative effects of vessel accelerations and make compensation for east and azimuth misalignment angle. Scholars establish the optimal function between the damping coefficients and variation of the east component of velocity error and then form an adaptive damping network with timely variable damping coefficients in Reference [11]. In this way, the abrupt change in damping coefficient is transformed into gradual change to make a smooth system status switch and overshoot errors can be effectively restrained. In Reference [12], an adaptive network-based fuzzy inference system (ANFIS) is proposed to adjust the damping ratio automatically in terms of the ship maneuver conditions. It says the ANFIS has nonlinearity and structured knowledge representation and can display immediate adaptive control and learning control behaviors. In Reference [13], an artificial damping loop is established and has the different damping coefficient from the actual one, which makes the Schuler oscillation phase of loop 2 advance that of loop 1 half a Schuler cycle. When the two loops work in parallel, Schuler oscillation errors within them will cancel each other out. As for the application of modern control theory, Reference [14] introduces a damping method based on Kalman filter. Through the foundation of the observation equation in both the internal damping state and the external damping state, the convergence time of Earth oscillation errors is shortened compared to the conventional damping method. In Reference [15], Kalman filter is applied in external horizontal damping algorithm for the shipborne grid SINS. It focuses on the influence of the constant error of Doppler Velocity Log (DVL) within the navigation solution and gives a brief criterion of the state switching based on the difference of the observations between two adjacent moments changes. In Reference [16], extended Kalman filter (EKF) combined with the Adams explicit formula has great accuracy and effectiveness in terms of attitudes estimation and can be well applied in underwater gliders for a long time of period. In Reference [17], EKF assisted with Takagi-Sugeno fuzzy algorithm is proposed. Under this kind of computational intelligence, INS/DVL integrated system maintains high ability of self-adaptation on system structure and parameters during the online process of state estimation and prediction. In Reference [18], unscented Kalman filter (UKF) is introduced to avoid the higher order truncation error in EKF and estimation results show UKF improves the steady state precision and convergence speed to some extent and displays more excellent filtering performance than EKF. In Reference [19], fusion techniques are presented to combine the advantages of various filters, such as EKF and UKF. Final test shows it can provide accurate and stable navigation solution. In general, less attention has been paid to the switch timing between damping and non-damping status at present. It is known to us that ship's maneuver won't stimulate navigation errors if FOGC can adjust its working mode in time to follow the principle of Schuler oscillation. Therefore, if the FOGC gains the ability of adjusting its working state timely and accurately, it can be well applied to indicate attitudes for warships and ship-borne weapons during rapid mobilization. In a word, the value of finding the proper moment for FOGC to switch state is significant and waits to be discovered.

In this paper, we propose a novel method mostly for the search of the perfect switch timing when the ship enters into some maneuver conditions. First, voyage data is collected as input by the FOCG fixed on board and wavelet denoising technology is applied through data pre-processing in order to make the classification more distinct. Next, classification norms of damping status and non-damping one are established. Support vector machine (SVM), once well trained, is found very suitable for FOGC to determine under what kinds of circumstances should the main system switch into non-damping mode, or get the damping network back online. After many rounds of parameter adjustment, the trained SVM model which reaches the highest classification accuracy is obtained. Finally, we pick another route in the adjacent sea for the FOGC system to make real time predictions during the period of the ship's maneuver. Results show the switch timings can be recognized through our Wavelet-SVM method clearly and the method has a better performance in the time of ship's maneuver compared to the whole-course damping network solution.

The remainder of this paper is divided into five sections: Section 2 presents the structure of the gyrocompass alignment loops and explains why a proper switch timing is vital in navigation's mode transformation. In Section 3, the method about dividing the whole voyage into different navigation stages is introduced in detail. In order to verify the feasibility of the method combining SVM and wavelet denoising, data from another voyage is adopted and relevant simulation is performed in Section 4. Finally, the conclusions are drawn in Section 5.

II. THEORY OF GYROCOMPASS ALIGNMENT

A. THE STRUCTURE OF GYROCOMPASS ALIGNMENT LOOPS

The symbols used in this paper are defined as followed: b represents the body frame; i is an inertial frame; e stands for the earth fixed coordinate frame; n is the East-North-Up navigation frame; R is the radius of earth; g is gravity acceleration; Ω_{xy}^{z} indicates an angular velocity of x frame with respect to y frame resolved in z frame; C_x^y is a measured transformation matrix from x frame to y frame. ΔV_E denotes eastern velocity error and ΔV_N denotes northern velocity error; $\tilde{\Omega}_{ib}^{b}$ is the angular velocity measured by gyros along the body frame; $\tilde{f}^b$ is the output of accelerometers along the body frame; ∇_E is the zero bias of the equivalent east accelerometer

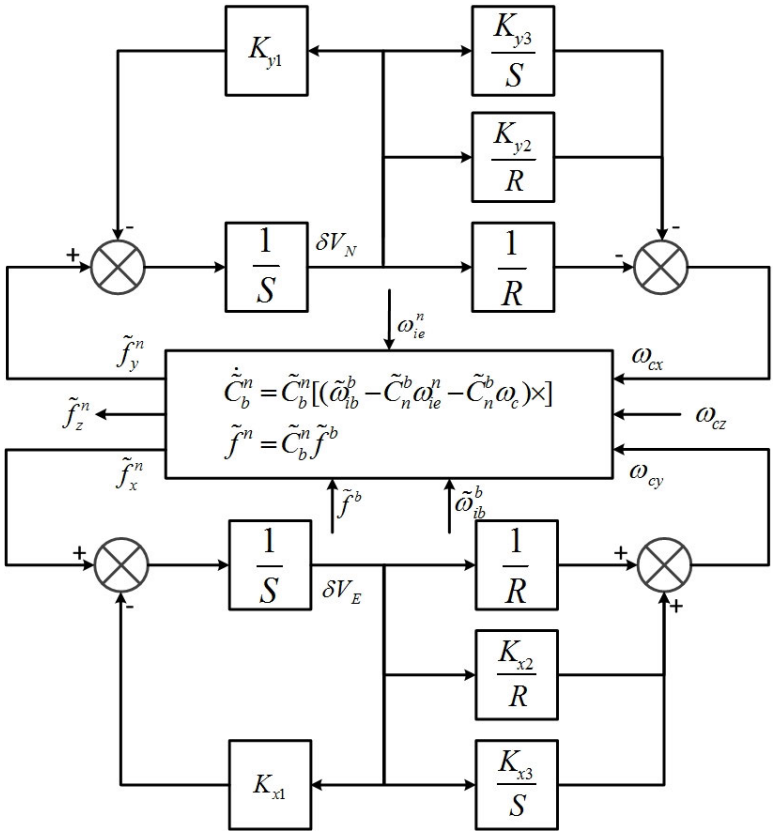

FIGURE 1. Block diagram of FOGC's horizontal alignment.

and ε_N is the equivalent north gyro constant drift. Finally, ϕ_N represents north misalignment angle.

Typical FOGC work procedure contains two steps. First, the leveling method, which is shown in Fig. 1, is both applied in eastern closed loop and northern closed loop to make sure the horizontal attitudes accurate and stable. Originally, when the inertial system is not equipped with those alignment loops, it has the characteristic equation as

$$\Delta(s) = s^2 + \omega_s^2 \tag{1}$$

where Ω_s represents Schuler frequency, we can see that the inertial system is an unstable system. After K_{x1} and K_{y1} (K_1) is added and the inertia unit is formed, the characteristic equation becomes

$$\Delta(s) = s^2 + K_1 s + \omega_s^2 \tag{2}$$

When $K_1 > 0$, the system is damped and tends to be stable. But the damping period is not decreased and it remains 84.4 minutes. Then we introduce K_{x2} and $K_{y2}(K_2)$ to fasten the leveling process. The equation can be written as

$$\Delta(s) = s^2 + K_1 s + (1 + K_2)\,\omega_s^2 \tag{3}$$

One more thing, the steady state error interfered with gyroscope zero bias and azimuth misalignment angle although the system is already stable. So K_{x3} and $K_{y3}(K_3)$ is involved to make sure those disorders can be eliminated. Finally, the characteristic equation is described as

$$\Delta(s) = s^3 + K_1 s^2 + (1 + K_2)\,\omega_s^2 s + RK_3\omega_s^2 \tag{4}$$

To ensure the stability, eigenvalues of (4) are set as

$$s_1 = -\sigma,\ s_{2,3} = -\sigma \pm j\omega_d \tag{5}$$

Then (4) can be rewritten as

$$(s + \sigma)\left(s + 2\sigma s + \sigma^2 + \omega_d^2\right) = 0 \tag{6}$$

Assuming that the second-order polynomial in (6) is a standard second-order system

$$(s + \sigma)\left(s^2 + 2\xi\omega_n s + \omega_n^2\right) = 0 \tag{7}$$

where Ω_n^2 is the system's resonant frequency, ξ is the damping ratio. Comparing (6) with (7),we can get

$$\omega_d^2 = \sigma^2\left(\frac{1}{\xi^2} - 1\right) \tag{8}$$

Substituting (8) into (6),we can get

$$(s + \sigma)\left(s + 2\sigma s + \frac{\sigma^2}{\xi^2}\right) = 0 \tag{9}$$

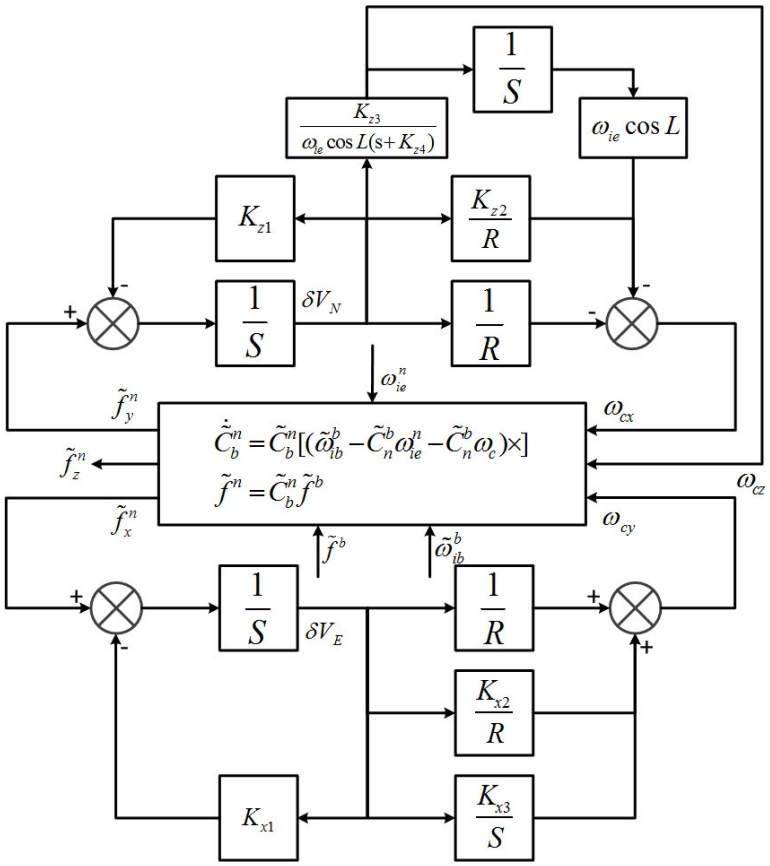

FIGURE 2. Block diagram of FOGC's azimuthal alignment.

Comparing (9) with (4),system parameters from level alignment loops can be obtained as follows:

$$\begin{cases} K_1 = 3\sigma \\ K_2 = \dfrac{\sigma^2}{\omega_s^2}\left(2+\dfrac{1}{\xi^2}\right)-1 \\ K_3 = \dfrac{\sigma^3}{g\xi^2} \end{cases} \tag{10}$$

In this way, K_1,K_1 and K_1 are determined by σ and ξ. According to Fig. 1, commanded angular velocities Ω_c are calculated through three-order alignment loops and therefore cause an influence on the final attitude matrix's determination:

$$\dot{\tilde{C}}_b^n = \tilde{C}_b^n\left[\left(\tilde{\omega}_{ib}^b - \tilde{C}_n^b\omega_{ie}^n - \tilde{C}_n^b\omega_c\right)\times\right] \tag{11}$$

Based on the leveling process, horizontal attitude angles are constantly updated and will tend to be stable, which makes preparations for the next stage: the azimuthal alignment.

When it comes to the azimuthal alignment, the east closed loop mentioned above remains the same but the north closed loop needs to make a few changes. Generally speaking, the gyrocompass is designed to find north automatically through collecting timevarying signals of inertial components and making corresponding commands. That is: when azimuth misalignment angle is generated, the north component of the angular velocity of earth rotation can be detected by the east gyroscope in some degree, which will cause the platform inclined relative to the horizontal level and it will bring an obvious change in the output of the north accelerometer. Therefore, those error terms eliminated by (4) now provide valuable information for the azimuthal alignment control. Therefore a four-order azimuthal alignment closed loop is newly built, which is shown in Fig. 2.

The characteristic equation of the azimuthal alignment closed loop is described as

$$s^4 + (K_{z1}+K_{z4})\,s^3 + \left[\omega_s^2\,(1+K_{z2}) + K_{z1}K_{z4}\right]s^2 + \omega_s^2\,(1+K_{z2})\,K_{z4}s + K_{z3}g = 0 \tag{12}$$

Assuming (4) can be rewritten as

$$\left[s^2 + 2\sigma s + \left(\sigma^2+\omega_d^2\right)\right]^2 = 0 \tag{13}$$

Substituting (8) into (12),we can get

$$\left(s + 2\sigma s + \frac{\sigma^2}{\xi^2}\right)^2 = 0 \tag{14}$$

Suppose that K_{z1} and K_{z4} have the same value and comparing (12) with (14), system parameters from level alignment

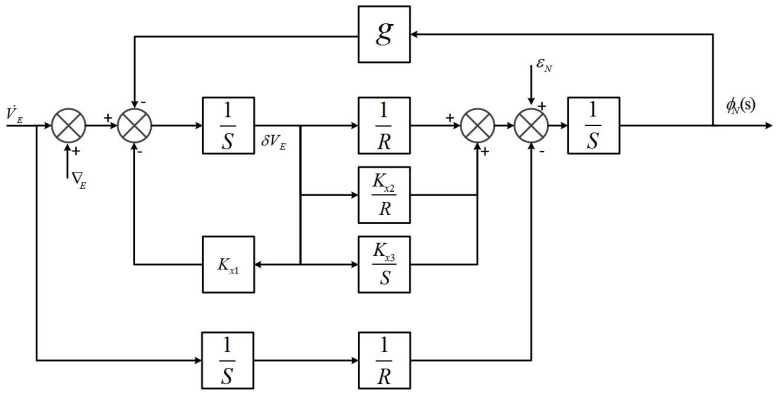

FIGURE 3. Error propagation diagram of the east closed loop 1.

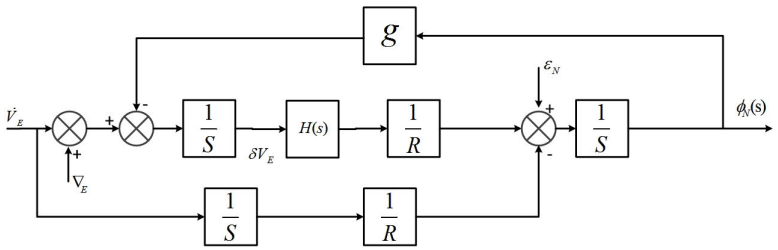

FIGURE 4. Error propagation diagram of the east closed loop 2.

loops can be obtained as follows:

$$\begin{cases} K_{z1} = 2\sigma \\ K_{z2} = \dfrac{2\sigma^2}{\xi^2\omega_s^2} - 1 \\ K_{z3} = \dfrac{\sigma^4}{g\xi^4} \\ K_{z4} = 2\sigma \end{cases} \tag{15}$$

Similarly, K_{z1}, K_{z2}, K_{z3} and K_{z4} are determined by σ and ξ. Through (11), the azimuth compensation is realized by the attitude matrix's update.

B. ANALYSIS ON FOGC'S OVERSHOOT ERRORS

To better understand gyrocompass alignment loops, our analyses above are established under static mode. In fact, most FOGCs work on in-motion platforms like ships and vehicles. Sudden velocity change caused by wide turns or acceleration will trigger overshoot errors in attitudes. Here we give some brief interpretations on overshoot errors caused by gyrocompass damping mode. Suppose the ship is sailing on the sea and the FOGC works in full damping mode. The error propagation diagram of the east closed loop is shown in Fig. 3.

Then we can obtain:

$$\frac{1}{s}\left\{\left[\dot{V}_E + \nabla_E - g\phi_N(s)\right]\frac{1}{s+K_{x1}}\left(\frac{1+K_{x2}}{R} + \frac{K_{x3}}{s}\right) + \varepsilon_N - \frac{\dot{V}_E}{sR}\right\} = \phi_N(s) \tag{16}$$

To simplify (16), we set

$$\frac{H(s)}{Rs} = \frac{1}{s+K_{x1}}\left(\frac{1+K_{x2}}{R} + \frac{K_{x3}}{s}\right) \tag{17}$$

Thus the error propagation block diagram in Fig. 3 can be redrawn in Fig. 4.

Fig. 4 is often called horizontal-damped navigation mode in traditional SINS. Therefore algorithms on level damp in SINS and FOGC are equivalent in essence.

From (16) and (17), we can get

$$\phi_N(s) = \frac{(H(s)-1)\dot{V}_B(s) + \nabla_E H(s) + \varepsilon_N Rs}{gH(s) + Rs^2} \tag{18}$$

Assuming system errors caused by gyro's constant drift and accelerometer's zero bias tend to be stable, we make some modifications of (18) and have

$$\phi_N(s) = \frac{H_x(s) - 1}{rs^2 + gH_x(s)}\dot{v}_E(s) \tag{19}$$

The duration of maneuvering is a small amount compared with Schuler cycle. Therefore acceleration of the ship within maneuver process can be treat as one kind of impulse input. According to Laplace law, we can get

$$\Delta v = \int_{t_1}^{t_2} \dot{v}_E(t)\mathrm{d}t \tag{20}$$

$$\dot{V}_E(s) = \Delta v \tag{21}$$

We plug (21) into (19) and then can have

$$\dot{V}_E(s) = \Delta v \tag{22}$$

If gyrocompass alignment loops do not exist, that is, the ship works in the non-damping mode and $H(s) = 1$. In this way, north misalignment angle won't be affected by east velocity change Δv. In other words, navigation systems employed with gyrocompass alignment loops or other level damp algorithms will suffer overshoot errors in attitudes when abrupt changes in ship's velocity are generated.

To avoid the harmful phenomenon mentioned above, the gyrocompass alignment loops should be cut off when the ship comes into the severe maneuver. By doing so commanded angular velocities in Fig. 2 won't contribute to the final transformation matrix's decisions and the navigation will switch into the normal inertial mode to resist external interference. However, this kind of undamped working state has the disadvantage of error accumulation and should be applied within a short term. After the maneuver condition, the gyrocompass alignment loops are back online again.

C. SHOWCASE OF IMPROPER WORKING STATE SWITCH AND ITS INFLUENCE

To demonstrate what consequences different state switch timings can cause, we conducted series of ship's maneuver beforehand with FOGC fixed on aboard. In the meantime, FOGC's output data and supplementary information such as log speed and ship's standard heading angle were collected simultaneously. Here we pick one of the maneuver conditions as an example. Fig. 5 shows the ship's velocity during the maneuver's time. Fig. 6 gives the ship's standard heading angle.

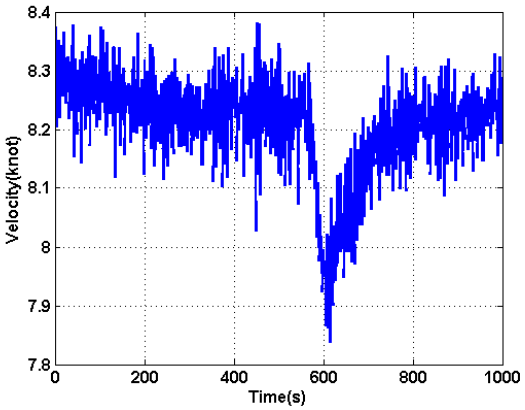

FIGURE 5. Forward velocity diagram of the ship.

Figs 5 and 6 illustrate that the ship experienced a turning maneuver and it led to dramatic changes in both velocity and heading angle. FOGC must adjust its working state to fit this situation. It requires FOGC to transform damping status into non-damping one to avoid error accumulation caused by the turning maneuver condition. This raises the question of the great choice of a proper switch timing. Here three FOGC navigation processes are illustrated with different switch timings. Each figure also uses the true head angles as a reference. Fig. 7 shows that the switch timing is set up as $t = 500s$.

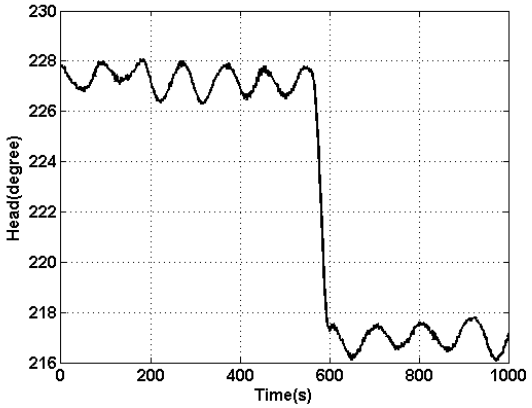

FIGURE 6. Heading angle diagram of the ship.

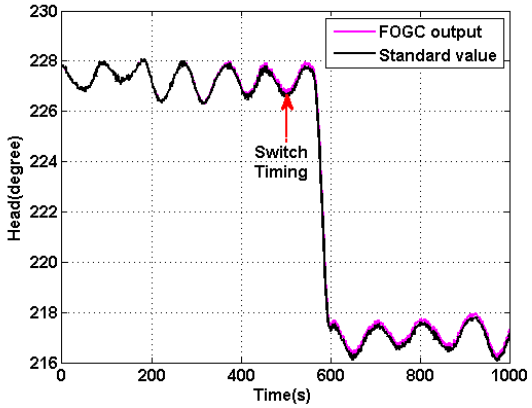

FIGURE 7. Heading angle diagram with switch timing of t = 500s.

In Fig. 9, the switch timing is set up as $t = 580s$. In Fig. 8, the switch timing is chosen right in the middle of the two in Fig. 7 and Fig. 9.

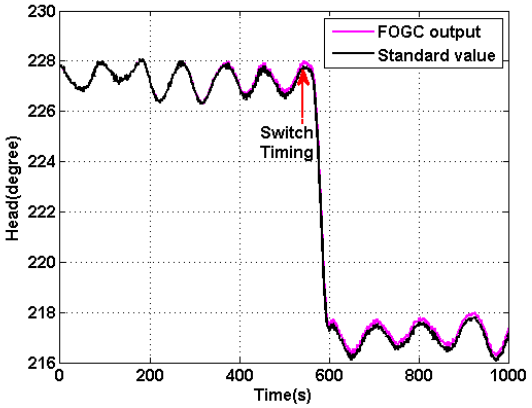

FIGURE 8. Heading angle diagram with switch timing of t = 540s.

To better reveal different results, we calculate heading errors respectively according to the three figures mentioned above and put them together in Fig 10. It is obvious that the switch timing of $t = 500s$ has excellent performance and the further ahead, the better. However,the actual changing decisions cannot be made that far in advance and must have a time

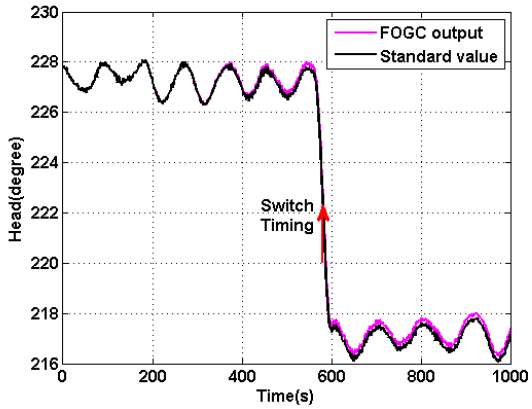

FIGURE 9. Heading angle diagram with switch timing of t = 580s.

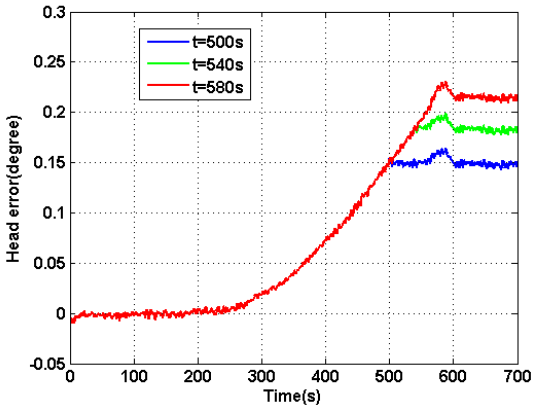

FIGURE 10. Comparison diagram of heading errors among different switch timings.

delay when the maneuver condition is perceived. The next chapter will explain how to make switch-timing decisions more intelligently in practical use.

III. CLASSIFICATION OF FOGC WORKING STATE BASED ON SVM

A. BRIEF INTRODUCTION OF SVM

SVM is a learning system widely used for data classification and regression. Compared to other discriminant functions, SVM has better performance in avoiding dimension curse and over-fitting problems [20]. It uses a hyperplane of liner functions to seperate different classes. The quality of classification is determined by the construction of the hyperplane. The optimal seperating hyperplane is the one that forms the largest margin between different types of training samples [21].

Consider a problem of seperating training samples into two training sets: (x_i, y_i) , $i = 1, 2, \ldots, N$; $y_i \in \{+1, -1\}$, where x_i is a feature vector and y_i is its class label. Then the optimal seperating hyperplane can be set as

$$w^T x + b = 0 \tag{23}$$

Once the parameters of w and b is determined, we can use two extreme lines to complete the classification:

$$\begin{cases} w^T x_i + b \geq +1, y_i = +1 \\ w^T x_i + b \leq -1, y_i = -1 \end{cases} \tag{24}$$

In the mean time, the margin can be maximized and calculated as $2/|w|$ [22].

The key to the classification is finding parameters of w and b of the optimal seperating hyperplane. SVM's constructing algorithms based on the optimization theory are listed bellow [23]:

$$\begin{aligned} &\min_{\alpha} \frac{1}{2} \sum_{i=1}^{l} \sum_{j=1}^{l} y_i y_j \alpha_i \alpha_j K\left(x_i, x_j\right) - \sum_{j=1}^{l} \alpha_j \\ &\text{s.t.} \sum_{i=1}^{1} y_i \alpha_i = 0 \\ &\quad 0 \leq \alpha_i \leq C, \quad i = 1, \cdots, l, \; j = 1, \cdots l \end{aligned} \tag{25}$$

where α_i represents the Lagrange multiplier, C is the penalty parameter and K is the kernel function.

After α_i is confirmed, we can get

$$w^* = \sum_{i=1}^{l} y_i \alpha_i^* x_i b^* = y_j - \sum_{i=1}^{l} y_i a_i^* K\left(x_i, x_j\right) \tag{26}$$

Finally the optimal separating hyperplane can be obtained

$$\left(w^* \cdot x\right) + b^* = 0 \tag{27}$$

And the decision function ia constructed as

$$f(x) = \operatorname{sgn}\left(\sum_{i=1}^{l} a_i^* y_i K\left(x_i, x_j\right) + b^*\right) \tag{28}$$

B. SVM'S APPLICATION ON VALIDATION OF THE SHIP'S DAMPING SWITCH TIMING

Since SVM shows great robustness and effectiveness in classification problems, it can also help us find the perfect switch timing when the ship performs emergency maneuver. Our priority is to divide the whole maneuver voyage into different time slots. However, most boundaries between those slots can be fuzzy and switch timings cannot be well confirmed. With the involvement of SVM, first we can use some periods of specific working state as training samples to complete the SVM's inner structure. Those time slots containing fuzzy boundaries can then be set as test samples. Finally, classification of working state can be distinct by using SVM's optimization algorithm through those test samples. The whole process of classification is illustrated in Fig. 11.

From Fig. 5 and Fig. 6 we can see that ship's forward acceleration and heading angular velocity are key features between steady voyage and maneuver voyage. In this way, we can make preliminary classification of some certain working state. Combining Fig. 5 and Fig. 6, it is convinced that time slot 1 from $t = 0s$ to $t = 200s$ is the period of steady voyage and the ship should work in the damping status. Similarly, time slot 3 from $t = 581s$ to $t = 700s$ is the period during which the ship should definitely work in the non-damping mode. Both time slots above can provide training data for the construction of SVM's inner network. Besides, we collect test data of time slot 2 from $t = 201s$ to

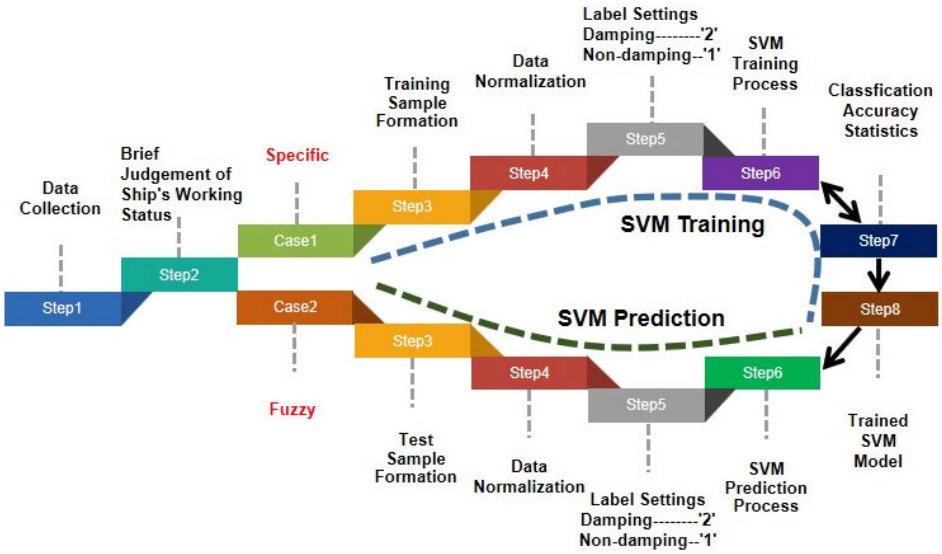

FIGURE 11. Flow diagram of SVM's classification procedure.

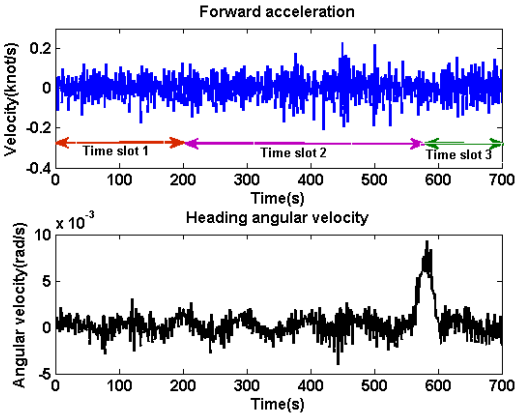

FIGURE 12. Brief classification of ship's working status.

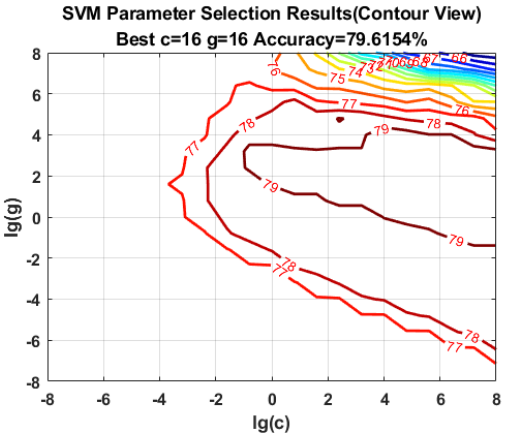

FIGURE 13. SVM parameter selection results(contour view).

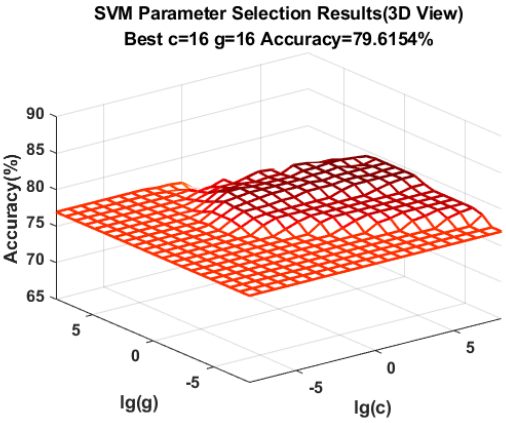

FIGURE 14. SVM parameter selection results(3D view).

$t = 580s$ because the switch timing most likely exists in that period and waits to be identified.

In this experiment, we use ship's forward acceleration and heading angular velocity to form feature vectors x_i. Class label collection is set as 1, 2, among which figure 2 represents damping working mode and figure 1 represents non-damping one. The kernel function uses the radial basis function and the SVM's inner network needs two key parameters to be verified, that is, the parameter g of the chosen kernel function and the penalty parameter c, the whole experiment cannot be conducted only once and it takes amounts of circulation to find the appropriate parameter combination until the classification accuracy achieves maximum value. Afterwards prediction based on the test data is carried out by means of reliable SVM's inner network. During optimization process, traversal search is applied and key parameters' discrete variables can be gradually determined in multiple cycles after setting their ranges respectively. Here are the optimization process of SVM's input parameters g and c illustrated in Fig. 13. and Fig. 14.

There may be many groups of g and c to fit the maximum accuracy. Our principle is to find the minimum value of c among those satisfactory groups. If the target we choose is not the only one with the minimum value of c. Then the

first satisfactory group generated during the optimization process is the one that will be employed. Finally, our optimization process reaches the highest accuracy of 79.6154% with the best selected parameters of $c = 16$ and $g = 16$. Next, we complete the prediction by the aid of newly built SVM's structure. Classification results are shown in Fig. 15. In Fig. 15, the switch timing of working status is $t = 565s$ and from that moment, FOGC should transfer from damping navigation mode into non-damping one.

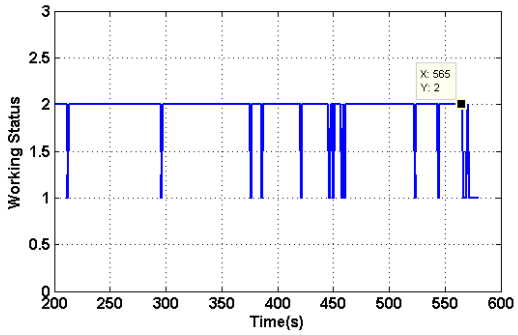

FIGURE 15. Test samples' classification results by SVM.

C. WAVELET DENOISING IN RAW DATA PREPROCESSING

It is obvious that interference factors exist in the final classification results which leads to several kicks in Fig. 15. This will interfere our judgement on the switch timing selection. Thinking the situation that the ship may subject to drastic changes in the external environment during the course, data samples we collected cannot come into use immediately and requires de-noising processing before data normalization in Fig. 11.

Wavelet analysis has the particular advantage in noise eliminating of signals and wide application foreground [25]. According to its time scale characteristic, wavelet analysis can approximate signals with most details such as edges, peaks and breakpoints well described [26], [27]. Here we pick wavelet denoising as the solution to the data preprocessing. Detailed procedures are given in Fig. 16.

FIGURE 16. Flow diagram of wavelet denoising's procedure.

Wavelet bases form the foundation of wavelet analysis, which are a series of sequence generated by the scaling and translation of a mother wavelet function [28]. Basically, a good choice of wavelet bases and decomposition layers is half success of wavelet denoising. Daubechies wavelet is often used for mutation signal detection, which fits well for our work to extract maneuver information. Among Daubechies wavelet family, wavelet bases "db3" and "db4" can take account of detection for both graded signals and jumping signals. Through our test, wavelet base "db3" is found more suitable for the following classification work. Next, it takes iterative experimentation to determine wavelet decomposition scale. Ideal decomposition scale can keep most useful components after signal decomposition and reconstruction process. After many trials, we finally select wavelet base "db3" to decompose the signals of forward acceleration and heading angular velocity to level 3 by MATLAB wavelet analysis toolbox. which is shown in Fig. 17. Figs 18 and 19 are decomposition pictures of forward acceleration and heading angular velocity respectively.

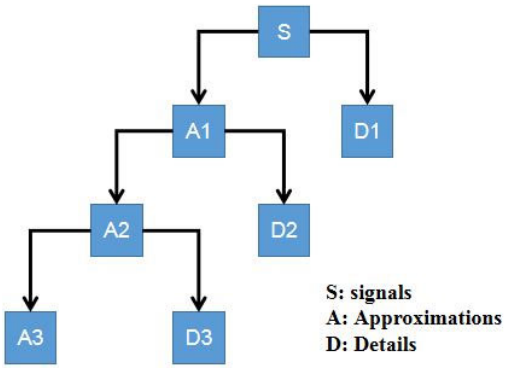

FIGURE 17. Structure of wavelet decomposition tree.

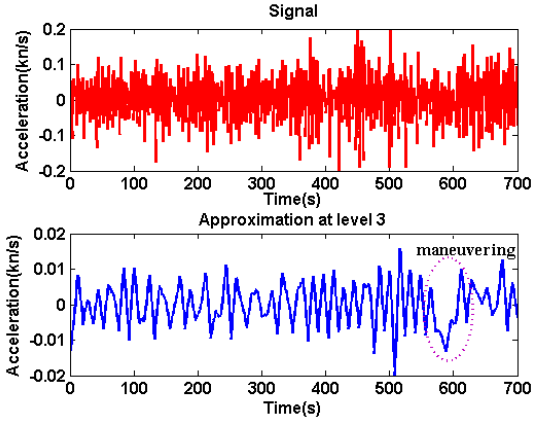

FIGURE 18. Decomposition results of forward acceleration.

Then we use data preprocessed with wavelet denoising as training and test samples of SVM's optimization experiment mentioned above. Through the operation flow shown in Fig. 11, this time our optimization process reaches the highest accuracy of 79.2308% with the best selected parameters of $c = 0.57435$ and $g = 5.278$. Parameter search results are illustrated in Fig. 20. and Fig. 21. Similarly, we use SVM recognition scheme to complete another round prediction, and modified classification results are shown in Fig. 22.

At last, classification of ship's working status has become more distinct and switch timing of $t = 565s$ is easy to be detected.

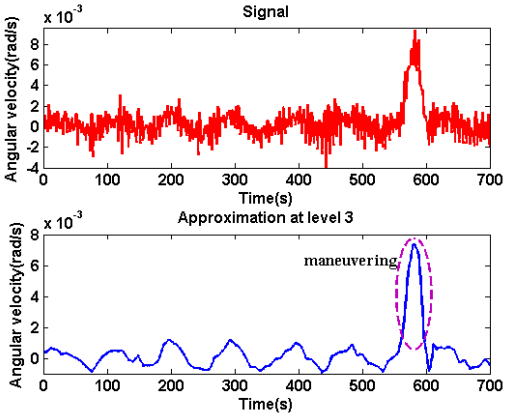

FIGURE 19. Decomposition results of heading angular velocity.

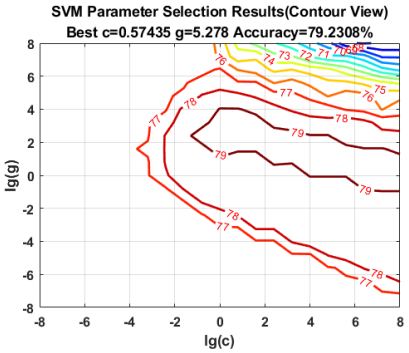

FIGURE 20. SVM parameter selection results(contour view).

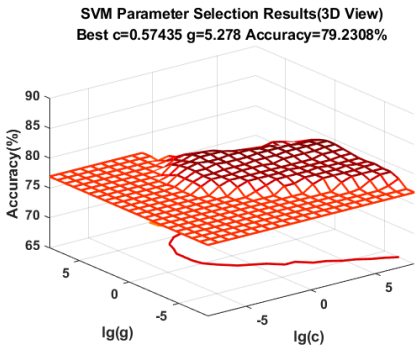

FIGURE 21. SVM parameter selection results(3D view).

D. COMPARISONS ON CLASSIFICATION RESULTS BY MEANS OF SEVERAL METHODS

In order to highlight our method's superiority, one traditional method of finding switch timing and BP neural network are introduced. As for the traditional method, if FOGC's system receives consecutive signals of dramatic heading angular velocity data in the pre-set time window, we think the ship comes across zigzag running conditions and FOGC should switch the damping working state immediately. But first the system need to collect enough data to distinguish which belong to high-dynamic voyage and which are not. Taking the same course shown in Fig. 6. as an example, we set

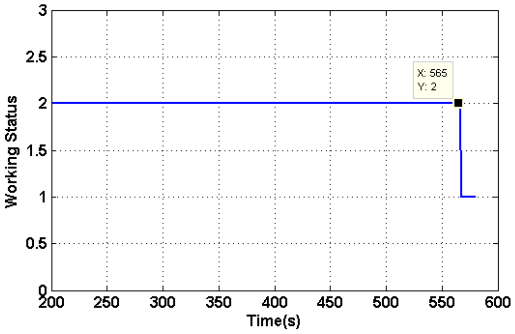

FIGURE 22. Modified test samples' classification results.

proper boundaries according to the value of heading angular velocities in Fig. 23.

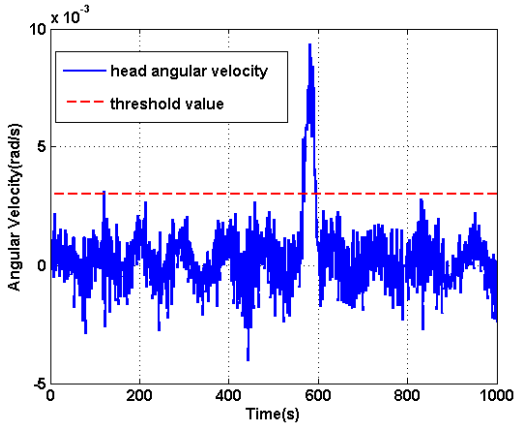

FIGURE 23. Predetermined limit based on the value of heading angular velocities.

If the condition is satisfied within the time window, the switch timing will be set once the window goes through. Finally we get three classification results by means of different methods, which are counted in Table 1. and Fig. 24.

TABLE 1. Classification result comparison among different methods.

Serial numbers	Methods	Switch timings
1	Wavelet-SVM	t=565s
2	Traditional method	t=569s
3	BP neural network	t=572s

Then we use those different switch timings to conduct three FOGC navigation calculations along the same voyage, and navigation results of heading attitudes are put together in Fig. 25.

From the picture above we can see that our Wavelet-SVM method has better performance during maneuvering navigation process. BP neural network has the most time delay. Traditional method may take a little advantage over BP neural network, but it is the most impractical way of detecting the switch timing. Because the range of the real heading angular velocity won't remain the same when the ship sails in different areas and make various zigzag maneuvers. So one must

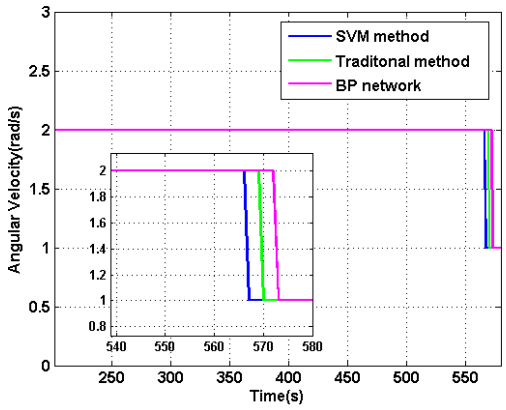

FIGURE 24. Classification result comparison among different methods.

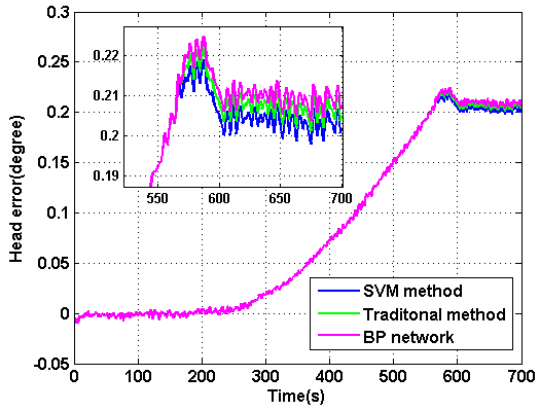

FIGURE 25. Heading attitude comparison resolved by different methods.

frequently adjust the threshold value of high-dynamic heading angular velocity in Fig. 23 when the ship comes across a new sailing condition. Due to the less dramatic maneuver we selected during the classification, Wavelet-SVM method's advantage in navigation accuracy may not show great obvious over the other methods.

IV. VERIFICATION OF WAVELET-SVM METHOD IN SWITCH TIMING IDENTIFICATION

A. NEW SAMPLE VALIDATION TEST BASED ON WAVELET-SVM METHOD

To further evaluate our method's feasibility, we choose another different course which contains several turning maneuver conditions. The experimental design is as follows: First our FOGC and SINS are parallel fixed in the bowels of the ship and have the same point as the ship's bow. GPS speed data are fully collected to simulate log speed, and so do the FOGC raw data and SINS raw data. Then we pick a river channel and make a ply voyage. Our experiment sailing route is shown in Fig. 26. FOGC, standard SINS and related supporting equipments are shown in Fig. 27. Fig. 28 gives the ship's velocity in one example of the maneuver conditions. Fig. 29 gives the ship's standard head attitude.

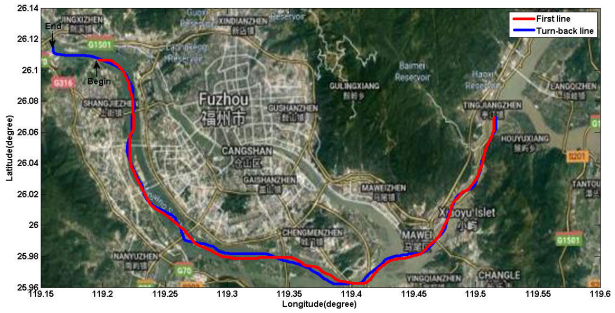

FIGURE 26. Experiment sailing route.

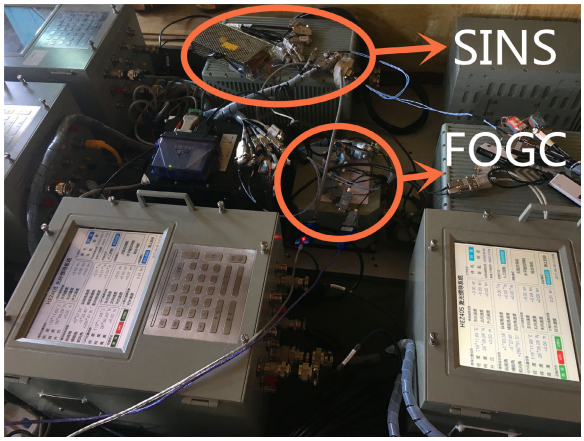

FIGURE 27. Experiment equipments.

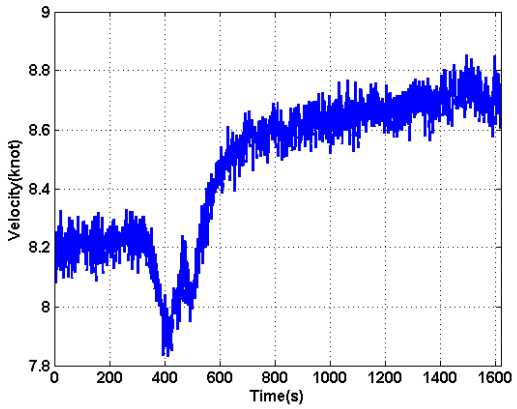

FIGURE 28. Forward velocity diagram of the ship.

Similarly We use Wavelet-SVM method to make classification of the FOGC's collected data. As the ship sails in the same area, we try not to train new samples and modify our SVM's model. In the optimization process, same class labels are adopted and predictions are made straightforward. The classification results during the whole voyage of this new selected turning maneuver are given in Fig. 30.

It can be seen that Wavelet-SVM method still work out the solution to distinguishing dynamic maneuver regions and making the right switch timings.

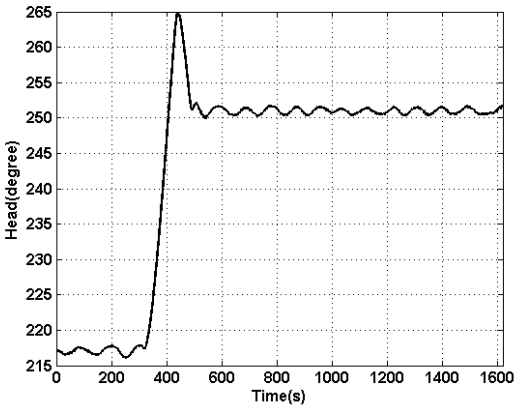

FIGURE 29. Heading angle diagram of the ship.

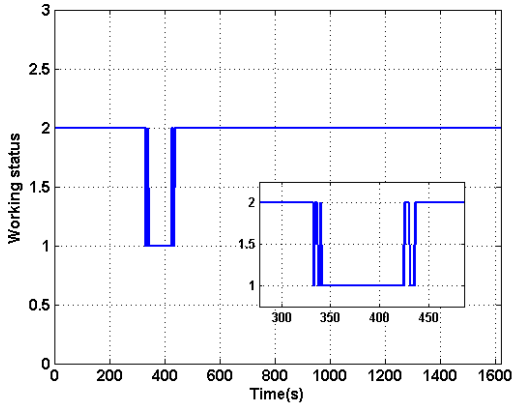

FIGURE 30. Classification results based on Wavelet-SVM method.

B. TEST RESULTS BASED ON THE WHOLE COURSE

We apply our trained model generated by Wavelet-SVM method into our FOGC navigation system and make comparisons to the all-time damping algorithm during full voyage process. Both heading attitude results together with standard heading attitudes are shown in Fig. 31.

It is obvious to see that there are several heading attitude overshoot times under traditional damping method during the whole voyage. Thanks to the in-time disconnection of damping loops by our Wavelet-SVM method, FOGC successfully avoids overshoot errors and maintain high precision north-finding function. In addition, we can see from the partial enlarged details that FOGC equipped with trained classification model has the advantage of quick response when dealing with zigzag maneuvering and its accuracy is closer to the true value.

V. VERIFICATION OF WAVELET-SVM METHOD IN SWITCH TIMING IDENTIFICATION

In order to evade overshoot errors caused by the damping network during on-sea maneuver conditions, people come up with the idea of cutting off FOGC's closed loop at the beginning of maneuvering and let it back online after dramatic changes. A novel method is proposed in this paper to help navigation systems automatically identify the best switch timings between damping and non-damping. Characterization data such as ship's forward velocity are collected in advance for SVM recognition scheme to form the classification model. Wavelet denoising is introduced in data preprocessing to make the classification model more accurate. After the Wavelet-SVM method make predictions of the ship's realtime working status, the optimal switch timings are easy to locate. With the switch timings well identified, FOGC can be precisely informed of sudden maneuver conditions and transfer into non-damping working state to slow down the error accumulation. Finally, the test examines the FOGC system north-finding capabilities and our Wavelet-SVM method show great performance over traditional damping algorithm both in overshoot error suppression and maneuver quick respond through the real ship. It is shown that, compared with the results from traditional threshold method, the switch

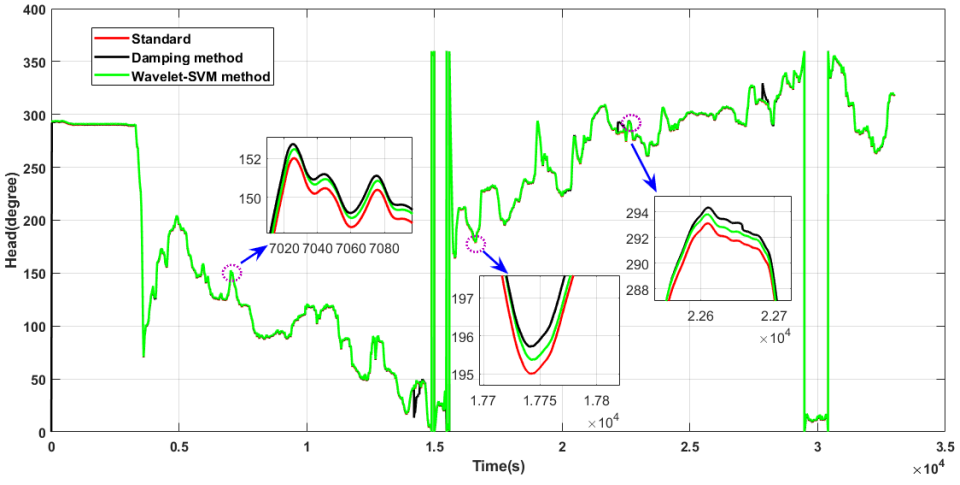

FIGURE 31. Whole-course heading attitude comparison resolved by different algorithms.

timing judgement is 4 seconds in advance, and compared with the results from all damping algorithm, the average heading error is reduced by 0.3 degree. In short, our method helps select the switch timing effectively and can be put into good use in modern ship navigation.

REFERENCES

[1] L. Zhang, W. Wu, M. Wang, and Y. Guo, "DVL-aided SINS in-motion alignment filter based on a novel nonlinear attitude error model," *IEEE Access*, vol. 7, pp. 62457–62464, 2019.
[2] L. Luo, Y. Zhang, T. Fang, and N. Li, "A new robust Kalman filter for SINS/DVL integrated navigation system," *IEEE Access*, vol. 7, pp. 51386–51395, 2019.
[3] S. Guo, J. Xu, and H. He, "External velocity aided coarse attitude and position alignment for dynamic SINS," *IEEE Access*, vol. 6, pp. 15099–15105, 2018.
[4] H. Won Park, J. Gyu Lee, and C. Gook Park, "Covariance analysis of strapdown INS considering gyrocompass characteristics," *IEEE Trans. Aerosp. Electron. Syst.*, vol. 31, no. 1, pp. 320–328, Jan. 1995.
[5] F. Sun, J. Xia, Y. Ben, and H. Lan, "Time-varying parameters based gyrocompass Alignment for marine SINS with large heading misalignment," in *Proc. IEEE/ION Position, Location Navigat. Symp. (PLANS)*, May 2014, pp. 1379–1383.
[6] R. Burns, "The use of artificial neural networks for the intelligent optimal control of surface ships," *IEEE J. Ocean. Eng.*, vol. 20, no. 1, pp. 65–72, Jan. 1995.
[7] Q. Li, Y. Ben, and F. Sun, "A novel algorithm for marine strapdown gyrocompass based on digital filter," *Measurement*, vol. 46, no. 1, pp. 563–571, Jan. 2013.
[8] S. Zhenyu, X. Jiangning, C. Muqing, W. Jie, and L. Houquan, "Integrated navigation system underwater and precision analysis used in synthetic aperture sonar motion compensation," in *Proc. 2nd Int. Conf. Signal Process. Syst.*, vol. 1, Jul. 2010, pp. 618–621.
[9] A. Asada and T. Ura, "Three dimensional synthetic and real aperture sonar technologies with Doppler velocity log and small fiber optic gyrocompass for autonomous underwater vehicle," in *Proc. Oceans*, Oct. 2012, pp. 1–5.
[10] F. Sun, J. Xia, Y. Ben, and Y. Zu, "A novel EM-Log aided gyrocompass alignment for in-motion marine SINS," *Optik*, vol. 126, no. 19, pp. 2099–2103, Oct. 2015.
[11] J. Sun, X. Xu, Y. Liu, T. Zhang, Y. Li, and J. Tong, "An adaptive damping network designed for strapdown fiber optic gyrocompass system for ships," *Sensors*, vol. 17, no. 3, p. 494, Mar. 2017.
[12] Q. Li, Y. Ben, and F. Sun, "Strapdown fiber optic gyrocompass using adaptive network-based fuzzy inference system," *Opt. Eng*, vol. 53, no. 1, Jan. 2014, Art. no. 014103.
[13] Q. Fangjun, H. Hongyang, and X. Jiangning, "Phase modulation-based SINS damping method for autonomous vehicles," *IEEE Sensors J.*, vol. 18, no. 6, pp. 2483–2493, Mar. 2018.
[14] L. Zhao, J. Li, J. Cheng, and Y. Hao, "Damping strapdown inertial navigation system based on a Kalman filter," *Meas. Sci. Technol.*, vol. 27, no. 11, Nov. 2016, Art. no. 115102.
[15] T. Fang, W. Huang, and L. Luo, "Damping rotating grid SINS based on a Kalman filter for shipborne application," *IEEE Access*, vol. 7, pp. 14859–14870, 2019.
[16] H. Huang, X. Chen, B. Zhang, and J. Wang, "High accuracy navigation information estimation for inertial system using the multi-model EKF fusing adams explicit formula applied to underwater gliders," *ISA Trans.*, vol. 66, pp. 414–424, Jan. 2017.
[17] S. Ansari-Rad, M. Hashemi, and H. Salarieh, "Pseudo DVL reconstruction by an evolutionary TS-fuzzy algorithm for ocean vehicles," *Measurement*, vol. 147, Dec. 2019, Art. no. 106831.
[18] M. Zhu, F. Yu, S. Xiao, and Z. Wang, "Research on gfsins/star-sensor integrated attitude estimation algorithm based on ukf," *Eng. Lett.*, vol. 26, no. 4, pp. 498–503, 2018.
[19] S. Cho, "IM-filter for INS/GPS-integrated navigation system containing low-cost gyros," *IEEE Trans. Aerosp. Electron. Syst.*, vol. 50, no. 4, pp. 2619–2629, Oct. 2014.
[20] C. Schuldt, I. Laptev, and B. Caputo, "Recognizing human actions: A local SVM approach," in *Proc. 17th Int. Conf. Pattern Recognit. (ICPR)*, vol. 3, 2004, pp. 32–36.
[21] G. Lu, H. Zhang, X. Sha, C. Chen, and L. Peng, "TCFOM: A robust traffic classification framework based on OC-SVM combined with MC-SVM," in *Proc. Int. Conf. Commun. Intell. Inf. Secur.*, Oct. 2010, pp. 180–186.
[22] J. Xu, W. Zeng, Y. Lan, J. Guo, and X. Cheng, "Modeling the parameter interactions in ranking SVM with low-rank approximation," *IEEE Trans. Knowl. Data Eng.*, vol. 31, no. 6, pp. 1181–1193, Jun. 2019.
[23] Y. Yang, J. Wang, and Y. Yang, "Exploiting rotation invariance with SVM classifier for microcalcification detection," in *Proc. 9th IEEE Int. Symp. Biomed. Imaging (ISBI)*, May 2012, pp. 590–593.
[24] X. Xuan, F. Bo, and W. Bo, "On-line realization of SVM Kalman filter for MEMS gyro," in *Proc. 3rd Int. Conf. Measuring Technol. Mechatronics Autom.*, vol. 2, Jan. 2011, pp. 768–770.
[25] C. Y. Guo and J. P. Li, "Development and future of wavelet analysis," in *Proc. 10th Int. Comput. Conf. Wavelet Active Media Technol. Inf. Process. (ICCWAMTIP)*, Dec. 2013, pp. 335–338.
[26] W. Boles and B. Boashash, "A human identification technique using images of the iris and wavelet transform," *IEEE Trans. Signal Process.*, vol. 46, no. 4, pp. 1185–1188, Apr. 1998.
[27] X. Li and J. Li, "Research on image digital watermarking based on wavelet transform and grey relational analysis," in *Proc. 10th Int. Comput. Conf. Wavelet Active Media Technol. Inf. Process. (ICCWAMTIP)*, Dec. 2013, pp. 162–166.
[28] Y. Lin, W. Chong-yang, and Z.-C. Wu, "Research on the selection of wavelet bases for wavelet-based signal trend elimination," in *Proc. Int. Conf. Wavelet Active Media Technol. Inf. Process. (ICWAMTIP)*, Dec. 2012, pp. 20–24.